Check for updates

A novel integration of a green power-to-ammonia to power system: Reversible solid oxide fuel cell for hydrogen and power production coupled with an ammonia synthesis unit

*Mulako Dean Mukelabai, Jonathon M. Gillard, Kumar Patchigolla**

School of Water, Energy and Environment (SWEE), Cranfield University, Cranfield, MK43 0AL, UK

HIGHLIGHTS

- P2A to power system enhances renewable energy usage by solving intermittency issues.
- Optimum P2A to power system design and operating parameters determined.
- Argon-free nitrogen resulting to non-limiting Haber Bosch recycle-loop fraction.
- Novel system has lowest reported ammonia synthesis electricity consumption.
- High power-to-ammonia efficiency attained, and excess ammonia available for market.

GRAPHICAL ABSTRACT
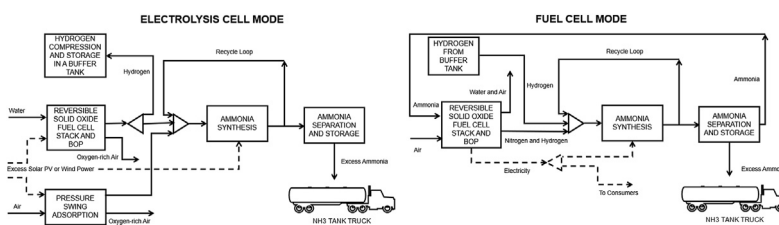
ARTICLE INFO

ABSTRACT

Renewable energy is a key solution in maintaining global warming below 2 °C. However, its intermittency necessitates the need for energy conversion technologies to meet demand when there are insufficient renewable energy resources. This study aims to tackle these challenges by thermo-electrochemical modelling and simulation of a reversible solid oxide fuel cell (RSOFC) and integration with the Haber Bosch process. The novelty of the proposed system is usage of nitrogen-rich fuel electrode exhaust gas for ammonia synthesis during fuel cell mode, which is usually combusted to prevent release of highly flammable hydrogen into the environment. RSOFC round-trip efficiencies of 41—53% have been attained when producing excess ammonia (144 kg NH₃/hr) for the market and in-house consumption respectively. The designed system has the lowest reported ammonia electricity consumption of 6.4—8.21 kWh/kg NH₃, power-to-hydrogen, power-to-ammonia, and power-generation efficiencies of 80%, 55—71% and, 64—66%.

* Corresponding author.
  E-mail address: k.patchigolla@cranfield.ac.uk (K. Patchigolla).

RSOFC
Modelling

Introduction

The world reliance on fossil fuels as the main source of energy has led to climate change and global warming. Renewable energy is seen as a key solution in maintaining global warming below 2 °C. The detrimental effects of climate change and global warming has propelled the world in the past decade into large-scale deployment of renewable energy technologies including wind, solar PV, concentrating solar power, biomass, etc. However, the intermittency of renewable energy, precisely solar irradiation and wind velocity, has necessitated the need for energy storage technologies to meet the energy demand when there is low or no solar irradiation and wind. The excess energy from solar PV or wind power can be stored and used later when there is no solar irradiation and wind.

Chemical energy storage technologies (power-to gas) such as electrolysers and fuel cells have gained attention with some technologies such as proton exchange membranes (PEM) being commercialised [1]. Power-to-gas-to-power systems are appealing because of high gas energy densities. High temperature reversible solid oxide fuel cells (RSOFC) have recently gained more attention because of their capability of electrolysis and fuel cell (power generation) operation in one single device. RSOFC has advantages over the conventional storage technologies in flexibility, adaptability, capability (versatility of power sizing and energy capacity in the two operation modes) and high efficiency [1]. The use of a single stack offers lower CAPEX through reduction in Balance of Plant components (BoP) since most of the components are used in both electrolysis and fuel cell operation.

However, hydrogen which is the main energy carrier envisaged in power-to-gas to power systems has huge storage and transportation costs related to its high flammability and low volumetric density while ammonia as a hydrogen carrier has low volumetric density and low flammability. Hydrogen is about 24 times more expensive to store compared to ammonia for one day storage (€/kg), 36 times more for 15 days storage and 28 times more for 182 days storage [2]. Consequently, hydrogen production and subsequent conversion into ammonia for energy storage has received a lot of attention because ammonia is viewed as the sustainable fuel (future liquid natural gas) to decarbonise the energy sector and the hard to abate industries. Ammonia is suitable for shipping to meet some of the energy demands currently met by LNG including power, transportation, heating, etc as well as its current use for fertiliser production.

Recently, there have been modelling studies on power-to-ammonia to power systems. Siddiqui and Dincer [3] developed a thermodynamic model of a solar based integrated energy system comprising of a solar PV plant, PEM electrolyser, pressure swing adsorption (PSA) unit, an ammonia synthesis unit and an ammonia fed alkaline fuel cell for power generation. The overall energetic and exergetic performance of the system varied through the year from 15.68 to 15.83% and 16.44–16.67% respectively. Rouwenhorst et al. [4] designed an islanded conceptual ammonia system for a location in northern Europe. The system consisted of wind and solar PVs for power generation, a battery, an electrolyser, a PSA for nitrogen production, an ammonia synthesis unit and a proton conducting ammonia fuelled SOFC for power generation. The system had a roundtrip efficiency of 61% while the energy consumption for ammonia production was 8.7–10.3 kW/kg NH$_3$.

Palys et al. [5] designed an ammonia based sustainable system for energy and agriculture. The system comprised of assumed Solar PV or Wind Turbines, an electrolyser, a PSA unit, an absorbent enhanced ammonia synthesis unit and hydrogen fed PEM and/or ammonia fuelled gensets. Ammonia fertiliser and fuel demands of 40,300 kg/year and an average hourly demand of 985 kW demonstrated the viability of the proposed system. Toyne and Schmuecker [6] designed and operate a renewable hydrogen and ammonia generation system comprised of a proton electrolyser, PSA, ammonia synthesis unit and ammonia fuelled tractors. The total energy consumption for ammonia synthesis is 13.895 kW/kg NH$_3$.

Wang et al. [7] investigated a power-to-x-to-power conceptual system with syngas, hydrogen, ammonia, methane and methanol. The power-to-hydrogen, power-to-ammonia, ammonia round-trip efficiency and hydrogen round-trip efficiency was 74%, 66%, 38.6% and 42.6% respectively. Ilbas et al. [8] developed a 3D numerical model of a tubular solid oxide fuel cell (SOFC) fed with ammonia in COMSOL. The results showed that the performance of ammonia fed SOFCs is comparable to those fuelled with hydrogen. Saadabadi et al. [9] carried out energy and exergy analysis of an ammonia fuelled SOFC integrated into a wastewater treatment plant. The net energy efficiency of the system with a heat pump assisted distillation was 39%.

Farhad and Hamdullahpur [10] designed a conceptual ammonia fuelled SOFC for power generation. The 100 W portable system had an efficiency of 41% with a cell voltage, operating voltage and fuel utilisation of 0.73 V, 25.6 V and 80% respectively. Al-Hamed and Dincer [11] developed a novel powering system that uses ammonia to produce power and hydrogen simultaneously to drive a passenger locomotive. The novelty of the on-board hydrogen production unit is the use of solid oxide fuel cell heat to disassociate hydrogen from ammonia with an overall energy efficiency of 61.2%. Ni [12] developed a 2D model of an ammonia fed thermo-electrochemical planar SOFC to investigate heat/mass transfer, ammonia cracking and electrochemical reactions. One of the model results showed that the temperature field is hardly affected by increasing the inlet gas velocity, but velocity reduction reduces the temperature gradient.

Tukenmez, Yilmaz and Ozturk [13] proposed a combined system driving a gas turbine cycle for seven useful outputs of power, hydrogen, ammonia, heating-cooling, drying and hot water. The energy efficiency of hydrogen production and the integrated plant is 57.92% and 62.18% respectively. Posdziech, Schwarze and Brabandt [14] showed the development of Sunfire's reversible solid oxide fuel cell technology. Their results showed the potential of the technology with fluctuating renewable energy sources. Aziz et al. [15] designed and integrated Nitrogen production, Ammonia synthesis, and power generation systems to convert Hydrogen to Ammonia. The highest total energy efficiency that they obtained is 66.92%, which includes an Ammonia production efficiency of 66.69% and a net power generation efficiency of 0.23%. Hauck, Herrmann and Spliethoff [16] presented and evaluated a thermodynamic model of a reversible solid oxide fuel cell. One of the parametric studies showed that increasing operation temperature and pressure can improve overall performance.

To the best of our knowledge, only one study considered the use of a RSOFC in the concept of power-to-ammonia to power system, without considering a detailed thermo-electrochemical model while all the other studies focus on ammonia utilisation in an SOFC, those studies that consider the use of SOFCs or fuel cells in general have not considered the use of an RSOFC. The studies that integrate fuel cells with an ammonia synthesis unit do not primarily focus on reducing the high energy consumption of ammonia synthesis, which will play a key role in utilisation of ammonia in the hydrogen and ammonia economy.

The aim of this study is to determine the optimum design and operating parameters to achieve a complete power-to ammonia to power system with just a single solid oxide cell stack, including full BoP components, using a detailed thermo-electrochemical model of an RSOFC developed in the commercial software Aspen Plus, validated through experimental results from literature. The novelty of this study is the way the RSOFC is integrated with an ammonia synthesis unit to establish synergies in the overall system that have not been previously established. By doing so it significantly drives down the ammonia synthesis energy consumption.

Process modelling

A 0-D model of the RSOFC was developed in the commercial software Aspen Plus as two subsystems; one for EC and one for FC operation. A nitrogen separation unit and an ammonia synthesis unit were modelled and integrated with the RSOFC. The model assumptions are:

- Isothermal reactor operation is assumed, outlet and inlet temperature of products and reactants is equal [17].
- Reactions immediately attain thermodynamic equilibrium due to the fast kinetics of equilibrium because of high operating temperature.
- The temperature of the RSOFC structure is assumed to be constant across the cell.

All the electrochemical equations used in RSOFC modelling are given in supplementary information section 1 according to

Refs. [16–24]. The anode and the cathode will be referred to as fuel and oxygen electrodes since the electrode polarities change when the stack is in fuel cell (FC) and electrolysis cell mode (EC) [25].

Solid oxide electrolysis stack

The SOEC stack developed is depicted in Fig. 1 where water at 298 K and 1.01325 bar is pumped as stream 1 through the fuel electrode side recuperator (FESRCP) where it is heated to 375 K by recovery of heat from fuel electrode gases (FEG) as they are cooled from 1113 K to 311 K, representing the minimum temperature beyond which there is cross flow in the recuperator. The water mixes with the hydrogen and steam from the fuel electrode gas recycle line (FEGRL) before being heated to the cell operating temperature of 1113 K in the heater (HTR-STM). The fuel electrode gases are cooled from 1113 K to 311 K in the recuperator. Water flow rate is determined by the desired stack current through a design specification block while stream 4 is maintained at 90% steam and 10% hydrogen by another design specification block by adjusting the fuel electrode recycle line (FEGRL) through a splitter to maintain reducing conditions at the fuel electrode [17]. The fuel electrode (FE) is modelled as a stoichiometric reactor where the steam is split into hydrogen gas and oxygen ions at a fractional conversion of 0.9. The oxygen ions migrate through the electrolyte (ELCTRLYT) to the oxygen electrode (OE) where oxidation takes place to form oxygen gas, which is removed by the sweep gas. Air at 293 K and 1.01325 bar is compressed in a three-stage compressor (SWPGCMP) to 298 K and 1.1 bar before heat is recovered from the oxygen electrode gas (OEG) stream in the oxygen electrode side recuperator (OESRCP) where it is heated to 1110 K representing the minimum pinch temperature of 3 K [26]. It is heated to the OE temperature of 1113 K in the heater (HTR-SWPG). The oxygen electrode gas stream is cooled from 1113 K to 621 K in the recuperator. Hydrogen in stream 10 is separated from the steam-hydrogen mixture in a separator (SEP) from where 75% of the pure hydrogen produced is compressed to 4 bar in a five-stage compressor and stored in a tank at 293 K, while the remainder is channelled to the Haber Bosch process. The sweep gas to fuel flow ratio is kept at 0.8 [27] to minimise performance reduction due to hydrogen leakage from the fuel electrode and reduce material reaction [17].

Solid oxide fuel cell stack

The SOFC stack developed is shown in Fig. 2 where ammonia flows from a tank at 112 bar and 253 K and depressurised at the valve to 1.1 bar and 241 K, then heated to 1110 K in the fuel electrode side recuperator (FESRCP) by the fuel electrode gases (FEG) as they are cooled from 1113 K to 360 K in the recuperator. The ammonia is then heated to the cell operating temperature of 1113 K in the heater (HTR-NH3). Ammonia flow rate is determined by the desired stack current.

The fuel electrode is modelled as a stoichiometric reactor where ammonia is split into hydrogen and nitrogen over a Ni/YSZ fuel electrode with a thermal conversion of 99.996% [28]. No Nitric oxide formation is assumed based on the experimental results of [28–30]. Oxygen ions transported from the
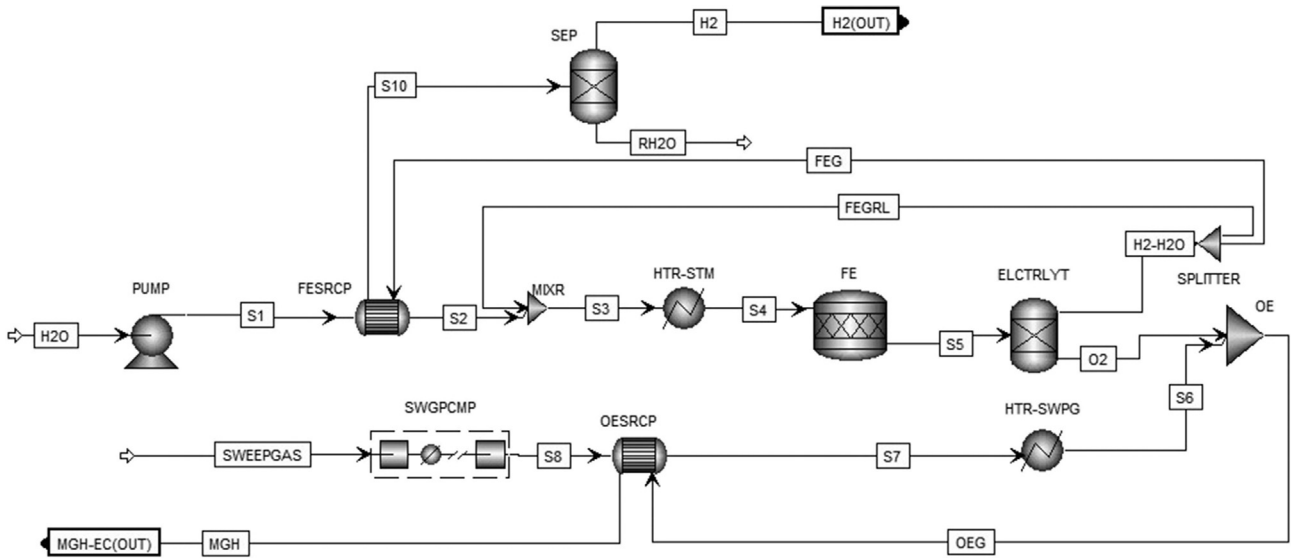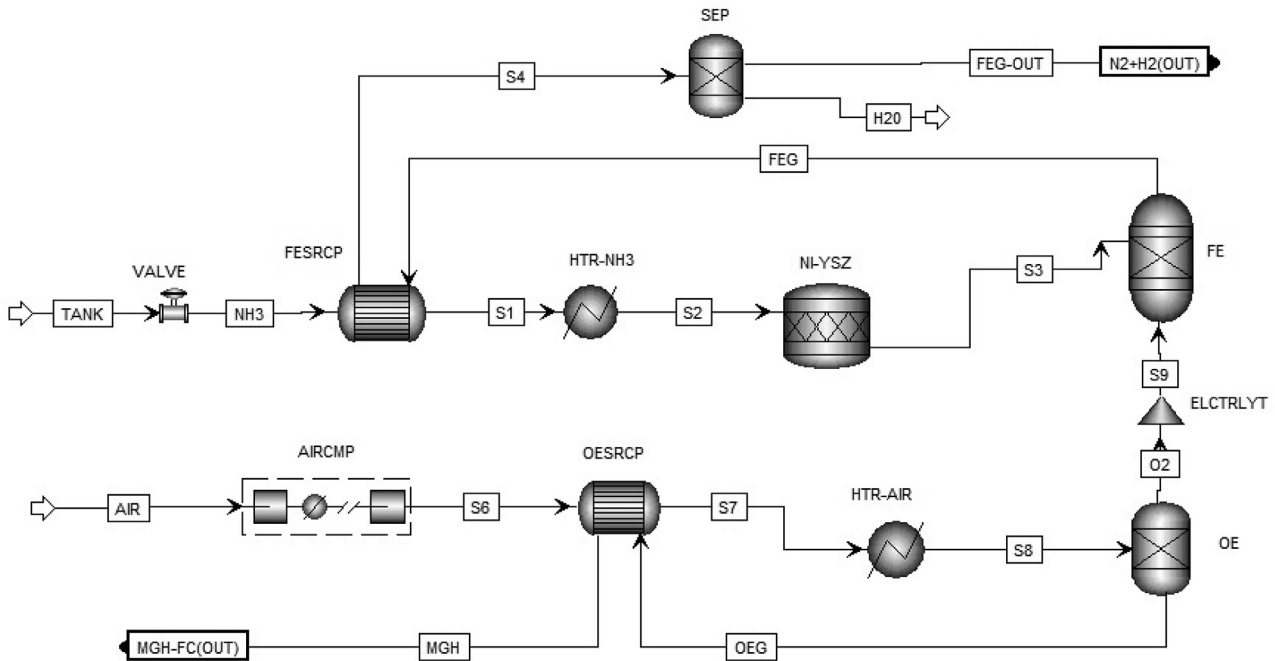
Fig. 1 — SOEC stack and BoP.

Fig. 2 — SOFC stack and BoP.

oxygen electrode (OE) through the electrolyte (ELCTRLYT) to the fuel electrode (FE) to form steam with hydrogen. Water separated from the FEG in the water trap modelled as a separator (SEP) maybe be stored for later reuse in electrolysis.

Air at 293 K and 1.01325 bar is compressed in a three-stage compressor (AIRCMP) to 298 K and 1.1 bar before being heated to 1027 K by the oxygen electrode gas (OEG) stream in the oxygen electrode side recuperator (OESRCP) where the oxygen electrode gases are cooled from 1113 to 301 K. The air is finally heated to the OE temperature of 1113 K in the heater (HTR-

AIR). The air flow to fuel flow ratio in real systems varies between 5 and 7 to remove the excess heat from the SOC stack [31]. In this model, the ratio was kept at 6 by using a design specification block.

RSOFC model performance parameters

Energy efficiency
In electrolysis, the power-to-hydrogen or energetic system efficiency is commonly defined as the ratio of energy output

from the hydrogen produced to the total energy input into the system [32], and is given by equation (1).

$$\eta_{power-to-hydrogen} = \eta_{sys,EC} = \frac{LHV_{H_2} \, n_{H_2}}{P_{el} + Q_{th} + Q_{H_2O} + \sum BoP_{EC}} \tag{1}$$

where LHV_{H_2} is the lower heating value of hydrogen (242.305 kJ/mol), n_{H_2} is the molar flow rate of hydrogen (mol/s), P_{el} and Q_{th} are the electric power and thermal energy required to split water (kW). Q_{H_2O} (kW) is the heat required to raise the steam to the operating temperature and $\sum BoP_{EC}$ (kW) is the total energy consumption of the RSOFC BoP components.

Similarly, power-to-ammonia is the ratio of energy output from the ammonia produced to the total energy input given by equation (2).

$$\eta_{power-to-ammonia} = \eta_{sys,EC} = \frac{LHV_{NH_3} \, n_{NH_3}}{P_{el} + Q_{th} + Q_{H_2O} + \sum BoP_{EC} + \sum BoP_{HB}} \tag{2}$$

where LHV_{NH_3} is the lower heating value of ammonia (316.7766 kJ/mol), n_{NH_3} is the molar flow rate of ammonia (mol/s) and $\sum BoP_{HB}$ (kW) is the total energy consumption of Haber Bosch process BoP components.

The power generation or energy efficiency in fuel cell mode is described as the ratio of the power generated to the energy input of the system, equation (3), [33].

$$\eta_{power\ generation} = \eta_{sys,FC} = \frac{P_{AC} - \sum BoP_{FC}}{n_{NH_3} M_{NH_3} LHV_{NH_3}} \tag{3}$$

where P_{AC} is the AC power generated (kW), M_{NH_3} is the molar mass of ammonia (mol/kg), LHV_{NH_3} is the ammonia lower heating value (18.6 MJ/kg), and n_{NH_3} is the molar flow rate of ammonia (mol/s). The ammonia production efficiency is calculated by equation (4).

$$\eta_{NH_3} = \frac{M_{NH_3} LHV_{NH_3}}{M_{H_2} LHV_{H_2}} \tag{4}$$

where M_{NH_3} is the mass flow rate of ammonia produced (kg/s) and M_{H_2} is the Haber Bosch hydrogen feed flow rate (kg/s).

Round trip efficiency

The roundtrip efficiency in terms of a reversible solid oxide cell can be described as the ratio of the net energy produced from the system during fuel cell mode to the net energy consumed during electrolysis cell mode and is given by equation (5).

$$\eta_{RT} = \frac{P_{FC,net}}{P_{EC,net}} = \frac{P_{AC} - \sum BoP_{FC}}{P_{el} + Q_{th} + \sum BoP_{EC} + \sum BoP_{HB}} \tag{5}$$

The roundtrip efficiency may slightly overestimate the efficiency since it does not take into consideration the energy variations that occur when switching from FC mode to EC mode and vice-versa. An inverter efficiency of 92% was used. Equations (1)–(5) including the electrochemical modelling equations in supplementary material were coded using Fortran language in Aspen Plus calculator blocks.

Model validation

SOEC
The SOEC was validated with the experimental results of Schefold, Brisse and Poepke [34]. Table S-2 in supplementary materials shows the simulation validation parameters. Activation energies, pre-exponential factors, porosity and tortuosity were obtained from Buttler et al. [21] since similar cell geometries were used in the two studies [16]. Fuel and oxygen electrode thicknesses were obtained from Hauck, Herrmann and Spliethoff [16]. The simulation results are in good agreement with the experimental results as can be seen in Figure S-1. The lowest and highest relative errors are 0.17% and 5.68% respectively.

SOFC
The SOFC was validated with the empirical results of Kazempoor and Braun [27]. The fitted simulation input parameters from Hauck, Herrmann and Spliethoff [16] and gas compositions are given in Table S-3, supplementary material. The simulation results fitted the experimental results very well as can be seen in Figure S-2, supplementary material. The lowest and highest relative errors are 0.08 and 6.4% respectively.

Air separation unit, ammonia synthesis unit and integrated model

An air separation unit was modelled as a simplified pressure swing adsorption unit, and an ammonia synthesis unit was modelled using the Haber Bosch process. These, including the integrated model are given in supplementary material in sections 4, 5 and 6. The model input and operating parameters are given below in Table 1. Optimisation and determination of the operating parameters is given in supplementary material sections 7 and 8.
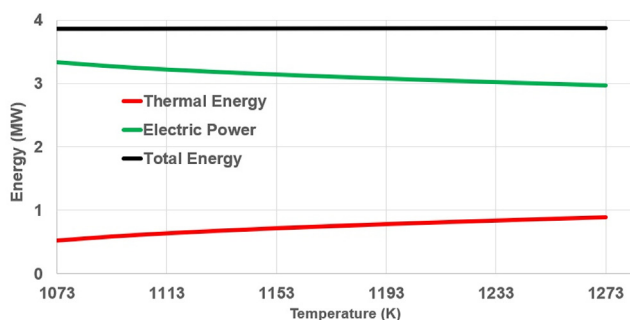
Results and discussion

Energy requirements

A sensitivity analysis of temperature against energy requirements in electrolysis is shown in Fig. 3 between 1073 K and 1273 K at a fixed current density of 0.6 A/cm². The electrical power required reduces from 3.3 to 3 MW while the thermal energy required increases from 0.5 MW to 0.9 MW as temperature increases. Operating at a higher temperature offers the advantage of attaining high efficiencies by providing external thermal energy required for water splitting through renewable thermal energy sources or waste heat recovery. No external heat would have been needed below 1113 K if the stack was operating a voltage close to thermal neutral voltage since overpotential heat is higher than thermal energy required for electrolysis [17,21, 32,35–37]. Parasitic load increment with temperature increment is only about 4.5% over the temperature range hence
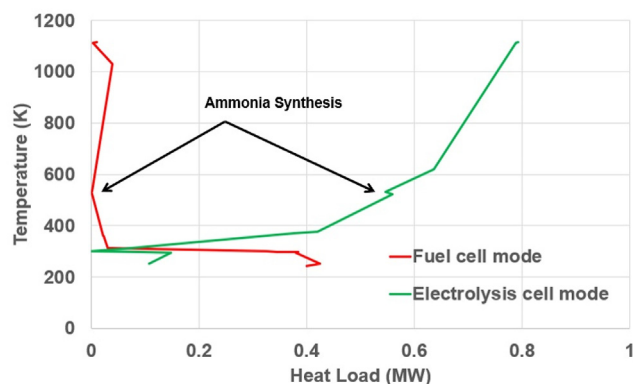
Table 1 – Model input parameters.

Parameter	Unit	Value	Parameter	Unit	Value
Stack Operation Temperature	K	1113	Air to Fuel Ratio$_{EC}$	–	0.8
Stack Operation Pressure	bar	1.1	Air to Fuel Ratio$_{FC}$	–	6
Water Inlet Temperature	K	298	Active Cell Area	m^2	1
Air Inlet Temperature	K	293	Number of Cells	–	500
X_{H_2O}	–	1	Operation Single Cell Voltage$_{EC}$	V	1.08
X_{NH_3}	–	1	Operation Single Cell Voltage$_{FC}$	V	0.86
X_{O_2}	–	0.2096	Operation Current Density$_{EC}$	A/cm^2	0.6
X_{N_2}	–	0.7811	Operation Current Density$_{FC}$	A/cm^2	0.45 – 0.56
X_{Ar}	–	0.0093	Haber Bosch Pressure	bar	112
$\dot{n}_{H_2O}$	kg/h	1108	Haber Bosch Temperature	K	533
$\dot{n}_{NH_3}$	kg/h	568 – 712	PSA Pressure	bar	20
$\dot{n}_{Air,PSA}$	kg/h	175.2	ΔP Through Components	bar	0
Fuel Utilisation$_{FC}$	–	100%	Minimum Pinch	°C	3
O$_2$ Utilisation$_{FC}$	–	50%	Isentropic Efficiency	–	88%
Fuel Utilisation$_{EC}$	–	90%	Mechanical Efficiency	–	99.8%

Fig. 3 – Electrolysis energy requirements.

Fig. 4 – Grand composite curve during electrolysis cell (EC) mode at 0.6 A/cm² (hydrogen production and ammonia synthesis) and fuel cell (FC) mode at 0.45 A/cm² (power generation and ammonia synthesis).

insignificant in comparison to thermal energy increment of 41%. Effects of temperature and current density on over-potentials and energy efficiency are discussed in detail in the supplementary material.

However, 0-D models may have disadvantages such as underestimation or over estimation of performance and parameters including reactor temperature, fuel to air ratios, etc., despite having quick calculations and provision of enough information for thermodynamic model development [38]. Therefore, it is recommended to further investigate the RSOFC stack in a multi-dimensional model to understand internal constraints that could lead to reactor failure such as temperature gradients, overpotential heat generation and overall reactor heat transfer analysis.

The heat integration of the process chain during EC and FC modes is shown in Fig. 4. Schematic of the two modes is given in Fig. 9. The grand composite curve shows that in EC mode a significant amount of energy is required to heat the water to the cell operating temperature because the heat released by the ammonia synthesis reactor temperature is 533 K and therefore only sufficient for preheating the hydrogen and nitrogen. Ammonia synthesis indicated by the arrow on the graph has a self-sufficient process to process heat transfer region in EC mode. The Haber Bosch compressor and refrigerator electricity consumption is very low because the Haber Bosch is operating at 25.4% capacity and the minimum allowable capacity is 25% [39]. In FC mode, very little electricity is required to heat the ammonia to the cell operating
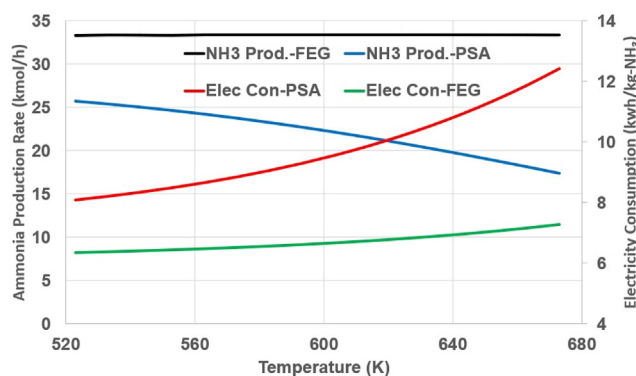
Fig. 5 – Effect of temperature on ammonia synthesis rate with nitrogen from fuel electrode gas (FEG) and PSA (pressure swing adsorption).

temperature because a signigicant amount of energy is recovered from the exiting fuel electrode gases and this is shown by the self-sufficient process to process heat transfer region above the pinch temperature. The high cooling duty required is due to refrigeration and compressor loads.
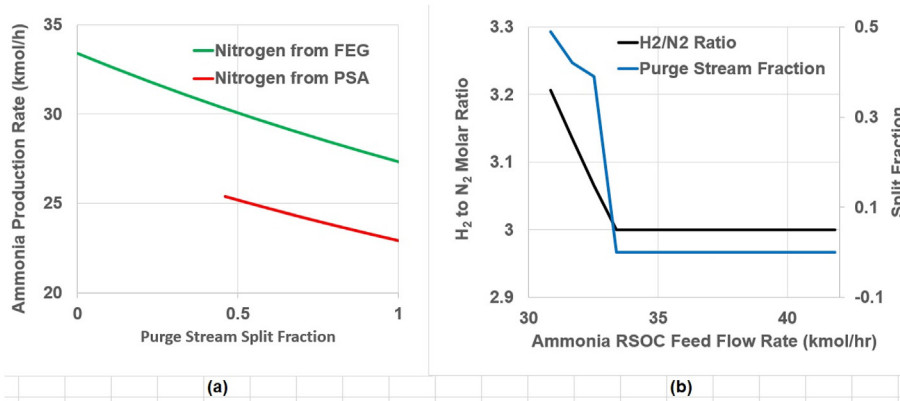
Fig. 6 – (a) Effect of purge stream split fraction on ammonia synthesis with argon-containing nitrogen from PSA and argon-free fuel electrode gas (FEG) (b) Effect of ammonia feed flow rate on hydrogen to nitrogen molar ratio and purge stream split fraction.

Hydrogen, power and ammonia synthesis

The novelty of the proposed system is the usage of nitrogen rich fuel electrode exhaust gas (FEG) for ammonia synthesis during FC mode, which is usually combusted to prevent release of highly flammable hydrogen into the environment. This nitrogen rich FEG can be directly used for ammonia synthesis during FC mode since it contains only 0.00092% ammonia while the ammonia synthesis recycle loop typically contains 4% ammonia [40]. In addition, several experimental studies have shown undetectable amounts of NOx formation in the fuel electrode. Dekker and Rietveld (2006) found that nitric oxide formation at 1223 K was only lower than 0.5 ppm while Ma et al. (2006, 2007) found undetectable amounts of nitric oxide at 1073 K. FEG stream contains only 1.2×10^{-10} mol.% NOx.

Figure 5 shows the effect of temperature on ammonia synthesis rate and DC energy over a temperature range of 523–673 K. Ammonia synthesis and DC energy consumption reduces and increases by only 0.0006 kmol/h and 0.9 kWh/kg NH_3 respectively when using nitrogen from fuel electrode gas. Ammonia synthesis and DC energy consumption reduces and increases significantly by 8.3 kmol/h and 4.3 kWh/kg NH_3 respectively when using nitrogen from PSA unit. Thus, using FEG for ammonia synthesis translates into higher ammonia synthesis rate and consequently low energy consumption per kg ammonia produced.

Figure 6(a) shows the effect of purge stream fraction on ammonia production rate when either fuel electrode gas and pressure swing adsorption derived nitrogen is fed to ammonia synthesis. The recycle loop fraction is non-limiting when nitrogen is fed from FEG for ammonia synthesis hence a higher ammonia production rate, as seen in Fig. 6(a), since there is no need for gas purging due to the absence of argon. When argon-containing nitrogen from PSA unit is used, the minimum recycle loop fraction is 0.54.

In Fig. 6(b), the effect of ammonia feed flow rate on molar ratio and purge stream fraction is investigated over the range of 30.8–41.8 kmol/h in FC mode. An Ammonia feed flow rate of 33.4 kmol/h represents the minimum flow rate at a current density of 0.45 A/cm². Beyond this value nitrogen becomes
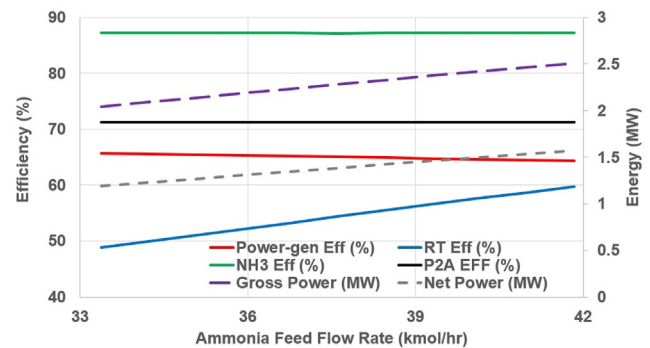
Fig. 7 – Effect of ammonia feed flow rate (kmol/h) on FC performance parameters, power generation efficiency (%), round-trip (RT) efficiency (%), power-to-ammonia (P2A) efficiency (%), ammonia production efficiency (%), Gross Power (MW), Net Power (MW).
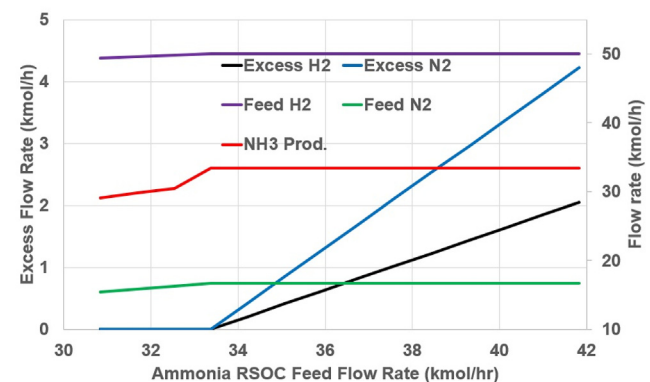
Fig. 8 – Effect of ammonia feed flow rate on system flow rates.

insufficient, the hydrogen to nitrogen molar ratio rises above 3 and equilibrium conditions cease to exist in the ammonia synthesis reactor leading to a reduction in ammonia production rate [40]. Industrial ammonia synthesis reactor conditions are usually maintained at 623–773 K, 100–300 bar,
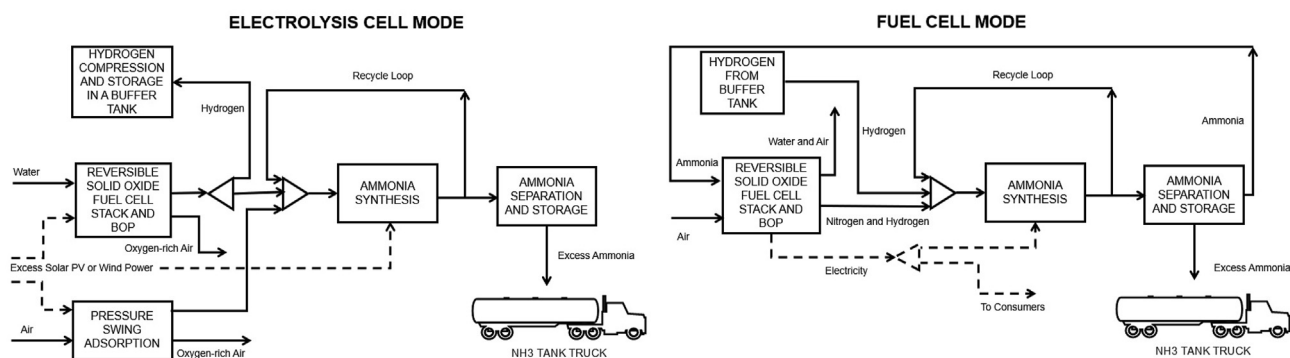
Fig. 9 – Schematic of electrolysis and fuel cell modes.

hydrogen to nitrogen molar ratios of 2:1–3:1 and inert gas composition of 0–15 mol% [41]. Feed flow rates above 33.4 kmol/h result in a molar ratio of 3 with a non-limiting recycle loop. When the ammonia synthesis reactor is fed with FEG the hydrogen to nitrogen molar ratio is not affected since the quantities of nitrogen and hydrogen are sufficient to maintain the molar ratio at 3:1, thus supporting equilibrium conditions in the ammonia synthesis reactor.

The effect of ammonia feed flow rate on gross power, net power, power generation efficiency, power-to-ammonia efficiency and ammonia production efficiency is shown in Fig. 7 at a fixed temperature of 1113 K. Gross power and net power increase from 1.9 to 2.5 MW, and 1.2–1.6 MW respectively as ammonia feed flow rate increases. Power generation efficiency slightly reduces from 66 to 64% as ammonia feed flow rate increases due to increment in parasitic load, while round trip efficiency increases from 41 to 53% since there is a significant increase in power generated as feed fuel flow increased. Power-to-ammonia and ammonia production energy efficiency remain constant at 71% and 87% respectively. Need for load-following is eliminated during FC mode since net power accounts for the ammonia energy consumption.

Figure 8 shows the effect of ammonia feed flow rate in FC mode on ammonia production hydrogen feed, ammonia production nitrogen feed, ammonia production, excess nitrogen and excess hydrogen flow rates. Hydrogen feed, nitrogen feed

and ammonia production rates are constant above an ammonia feed flow rate of 33.4 kmol/h despite the increment in feed flow rate. Excess nitrogen and hydrogen flow rates are zero up to 33.4 kmol/h, then begin to increase from 0 to 2.1 kmol/h respectively, as ammonia feed flow rate increases. Increasing ammonia feed flow rate above 33.4 kmol/h results to excess hydrogen and nitrogen which could be combusted to generate additional power. The minimum ammonia feed flow rate matches with the ammonia production rate of 33.4 kmol/h at an energy efficiency of 64% implying that the ammonia produced during EC mode, 8.5 kmol/h or 144 kg/h can be sold to the market. High ammonia production rate, non-limiting recycle-loop fraction, additional unreacted hydrogen from FEG and shutdown of PSA unit results in a very low total energy consumption of 6.41 kW/kg NH_3. An ammonia feed flow rate of 41.8 kmol/h represents the maximum flow rate that matches the total the ammonia produced during EC and FC modes. This could be used to maximise power production without producing excess ammonia for sale.

Ammonia synthesis energy consumption

Case 1: EC mode
Energy consumption analysis for ammonia production in EC mode is given in Table 2. Electricity consumption for water purification is 3 kWh/tonne-water through reverse osmosis

Table 2 – EC and FC ammonia energy consumption.							
EC ammonia energy consumption				**FC ammonia energy consumption**			
Component	Units	Value		Component	Units	Value	
Temperature	K	533	623	Temperature	K	533	623
P_{el}	kW	3218	3218	P_{el}	kW	3218	3218
Q_{steam}	kW	842.46	842.46	Q_{steam}	kW	842.46	842.46
$P_{ECCompressor}$	kW	3.16	3.16	$P_{ECCompressor}$	kW	3.16	3.16
$Q_{sweepgas}$	kW	1.38	1.38	$Q_{sweepgas}$	kW	1.38	1.38
P_{pump}	kW	0.0027	0.0027	P_{pump}	kW	0.0027	0.0027
$P_{WaterPurification}$	kW	3.32	3.32	$P_{WaterPurification}$	kW	3.32	3.32
25% hydrogen towards Haber Bosch ∴4065.25 × 0.25 = 1016.32				$P_{H_2 storage compression}$	kW	48	48
$P_{HBCompressor}$	kW	89.15	103.68	75% hydrogen from storage ∴4116.27 × 0.75 = 3087.2			
$Q_{HBHeater}$	kW	2.22	5.98	$P_{HBCompressor}$	kW	355.16	496.61
$Q_{HBCooler}$	kW	46.66	43.6	$Q_{HBHeater}$	kW	8.74	28.56
P_{PSA}	kW	29.12	29.12	$Q_{HBCooler}$	kW	183.93	208.33
$\dot{n}_{NH_3}$	kg/h	144.16	69.71	$\dot{n}_{NH_3}$	kg/h	568.42	568.4
DC Energy Consumption	**kWh/kg NH_3**	8.21	10.08	**DC Energy Consumption**	**kWh/kg NH_3**	6.4	6.74

Table 3 – Model output parameters.

Parameter	Unit	Value
P_{EC}	MW	3.2
P_{FC}	MW	$2 - 2.5$
$P_{NetPower,FC}$	MW	$1.1 - 1.4$
$\dot{n}_{H_2,total}$	kg/h	113
$\dot{n}_{N_2,PSA}$	kg/h	131
$\dot{n}_{N_2,FC}$	kg/h	$468 - 586$
$\dot{n}_{H_2,FC}$	kg/h	$16 - 20$
$\dot{n}_{NH_3,EC}$	kg/h	114
$\dot{n}_{NH_3,FC}$	kg/h	568
Power − to − H_2 Efficiency	%	80
Power − to − NH_3 Efficiency	%	$55 - 71$
Power − Gen Efficiency	%	$64 - 66$
Ammnia Synthesis Efficiency	%	79-87
Roundtrip Efficiency	%	$41 - 53$

[42]. Electrolysis energy consumption in EC mode is 25% of total electrolysis energy consumed since 25% of hydrogen produced is used in the Haber Bosch process while 75% is stored for use in FC mode. Energy consumption is calculated at a temperature of 533 K and 623 K. When a conventional iron-based catalyst is used for ammonia synthesis at temperatures of 623 K, ammonia synthesis rate and DC energy consumption for ammonia production are 69.7 kg/h and 10 kWh/kg NH_3 respectively. Conventional iron-based catalysts yield much lower reaction rates in the temperature range of 523–673 K than conventional ruthenium-based catalysts, which have higher activity in the range of 648–723 K but undergo hydrogen poisoning below 593 K [43]. Kitano et al. [43] developed a novel Ru/Ba−Ca(NH$_2$)$_2$ catalyst which experiences little hydrogen poisoning, has a high surface area and facilitates operation as low as 378 K.

Case 2: FC mode
In FC mode, 75% of hydrogen produced is stored in a buffer tank for use in the Haber Bosch process during FC mode. Therefore, electrolysis energy consumption is 75% of total electrolysis energy consumed. Energy consumption includes compression energy since stored hydrogen is compressed to 4 bar. Ammonia synthesis rate and DC energy consumption in FC mode at 533 K and 623 K are 568.4 kg/h, 6.41 kWh/kg NH_3 and 6.74 kWh/kg NH_3 respectively. This shows that either a conventional iron-based catalyst or a ruthenium-based catalyst could be employed in this system. A summary of the model output parameters is given in Table 3.

Conclusions

A power-to-ammonia to power system has been designed through thermo-electrochemical model development, simulation and validation through literature experimental results of a reversible solid oxide fuel cell stack along with BoP components integrated with the Haber Bosch process using the commercial software Aspen Plus. A renewable electricity source such as solar PV or wind farm is assumed to be readily available to provide electricity during electrolysis cell mode to produce hydrogen, which is converted to ammonia and subsequently used in fuel cell mode to generate power.

The system has power-to-ammonia and power generation efficiencies in EC and FC mode of 55–71% and 64–66% respectively. The system has roundtrip efficiencies of 41–53% with net power of 1.2 MW and 1.6 MW when ammonia is produced in excess for sale or consumed inhouse respectively. The novel system has the lowest ammonia electricity consumption reported of 6.41 kWh/kg NH_3 in FC mode and 8.21 kWh/kg NH_3 in EC mode, at ammonia production efficiencies of 79%−87% in EC mode and FC mode respectively. This is more efficient than a large-scale Haber Bosch process integrated with a PEM electrolyser (8.6−9.5 kWh/kg NH_3) and large-scale steam methane reforming-based plants (7.78−9.06 kWh/kg NH_3) which have efficiencies in the range of 62−65%.

The novelty of the proposed system is the usage of nitrogen-rich fuel electrode exhaust gas for ammonia synthesis during FC mode, which is usually combusted to prevent release of highly flammable hydrogen into the environment. Increased ammonia production rate, non-limiting recycle-loop fraction, unreacted hydrogen from the nitrogen rich exhaust gas mixture and shut down of the PSA unit during FC mode leads to a very low ammonia energy consumption rate. The system has shown remarkable synergies and advantages in flexibility, adaptability, capability and high efficiencies obtained. It can enhance renewable energy usage by either meeting local energy needs or connecting to a large-scale power grid to improve utilisation of solar PV or wind power plants and to stabilise the grid. Excess ammonia produced (144 kg NH_3/hr) can be sold to the market. Medium grade heat is available from the system which can be used for domestic/industrial heating or cooling purposes.

Funding

Declaration of competing interest

The authors declare that they have no known competing financial interests or personal relationships that could have appeared to influence the work reported in this paper.

Acknowledgements

Appendix A. Supplementary data

Supplementary data to this article can be found online at https://doi.org/10.1016/j.ijhydene.2021.02.218.

Nomenclature

A	Active cell area (m^2)
AC	Alternating current (A)
BoP	Balance of Plant
$CAPEX$	Capital Expenditure
DC	Direct current (A)
$D_{eff,m}$	Effective diffusion coefficient of gas species m (m^2/s)
$D_{kn,m}$	Knudsen diffusion coefficient of gas species m (m^2/s)
D_{m-n}	Binary diffusion coefficient between gas species m and n (m^2/s)
d_p	Average electrode diameter (m)
$E_{act,m}$	Activation energy of cell component (J/mol)
EC	Electrolysis cell mode
F	Faraday constant (C/mol)
FC	Fuel cell mode
ΔG	Change in Gibbs free energy (J/mol)
ΔH	Change in enthalpy of reaction (J/mol)
I	Cell operating current (A)
$j_{0,m}$	Exchange current density of electrode m (A/m^2)
LHV	Lower heating value (MJ/kg)
M_m	Molar mass of component m (g/mol)
n	Number of electrons transferred
$\dot{n}$	Molar flow rate (mol/sec)
N	Stack number of cells
P	Operating pressure (bar)
P_{elec}	Electric power (kW)
Q_{H_2O}	Heat transfer rate to steam (kW)
Q_{NH_3}	Heat transfer rate to ammonia (kW)
Q_{ohm}	Ohmic heat transfer rate generated (kW)
Q_{TH}	Thermal energy required to split water (kW)
R	Universal gas constant $(J/mol.K)$
r_{ohm}	Specific ohmic resistance (Ωm^2)
ΔS	Entropy change (J/mol)
T	Operating temperature (K)
U_F	Fuel utilisation
$V_{act,m}$	Activation overpotential of electrode m (V)
$V_{conc,m}$	Concentration overpotential of electrode m (V)
V_{ohm}	Ohmic overpotential (V)
V_{OP}	Operating voltage (V)
$V_{d,m}$	Diffusion volume of gas species m
x	Molar fraction
$\alpha_{a,m}$	Anodic transfer coefficient of electrode m
$\alpha_{c,m}$	Cathodic transfer coefficient of electrode m
ε	Electrode porosity
σ	Conductivity (Ωm^{-1})
$\sigma_{0,el}$	Electrolyte conductivity pre-exponential factor (Ωm^{-1})
$\gamma_{0,m}$	Activation overpotential pre-exponential factor for electrode m (A/m^2)
δ_m	Thickness of cell component m (m)
τ	Electrode tortuosity
η	System efficiency

REFERENCES

[1] Venkataraman V, Pérez-Fortes M, Wang L, Hajimolana YS, Boigues-Muñoz C, Agostini A, McPhail SJ, Maréchal F, Van Herle J, Aravind PV. Reversible solid oxide systems for energy and chemical applications — review & perspectives. J Energy Stor 2019;24(February):100782. https://doi.org/10.1016/j.est.2019.100782. Elsevier.

[2] Vrijenhoef JP. Decentralised ammonia production in The Netherlands. In: Proceedings of the 16th NH3 fuel conference. Los Angeles, USA; 2016. 20 September 2016, [California].

[3] Siddiqui O, Dincer I. A new solar energy system for ammonia production and utilization in fuel cells. Energy Convers Manag 2020;208(February):112590. https://doi.org/10.1016/j.enconman.2020.112590. Elsevier.

[4] Rouwenhorst KHR, Van der Ham AGJ, Mul G, Kersten SRA. 'Islanded ammonia power systems: technology review & conceptual process design'. Renew Sustain Energy Rev 2019;114(August 2019):109339. https://doi.org/10.1016/j.rser.2019.109339.

[5] Palys MJ, Kuznetsov A, Tallaksen J, Reese M, Daoutidis P. A novel system for ammonia-based sustainable energy and agriculture: concept and design optimization. Chem Eng Proc - Proc Intensification 2019;140(February):11—21. https://doi.org/10.1016/j.cep.2019.04.005. Elsevier.

[6] Toyne D, Schmuecker J. Our Iowa renewable hydrogen and ammonia generation system. In: Proceedings of the 14th annual NH3 fuel conference: enabling optimized, sustainable energy and agriculture, NH3 fuel association. Minneapolis, USA. MN: AIChE; 2017. 1-2 November 2017.

[7] Wang L, Zhang Y, Pérez-Fortes M, Aubin P, Lin T, Yang Y, Maréchal F, Van herle J. Reversible solid-oxide cell stack based power-to-x-to-power systems: comparison of thermodynamic performance. Appl Energy 2020;275(February):115330. https://doi.org/10.1016/j.apenergy.2020.115330. Elsevier.

[8] Ilbas M, Kumuk B, Alemu MA, Arslan B. Numerical investigation of a direct ammonia tubular solid oxide fuel cell in comparison with hydrogen. Int J Hydrogen Energy 2020;45(60):35108—17. https://doi.org/10.1016/j.ijhydene.2020.04.060. Elsevier Ltd.

[9] Saadabadi SA, Patel H, Woudstra T, Aravind PV. Thermodynamic analysis of solid oxide fuel cell integrated system fuelled by ammonia from Struvite precipitation process. Fuel Cell 2020;20(2):143—57. https://doi.org/10.1002/fuce.201900143.

[10] Farhad S, Hamdullahpur F. Conceptual design of a novel ammonia-fuelled portable solid oxide fuel cell system. J Power Sources 2010;195(10):3084—90. https://doi.org/10.1016/j.jpowsour.2009.11.115.

[11] Al-Hamed KHM, Dincer I. A novel ammonia solid oxide fuel cell-based powering system with on-board hydrogen production for clean locomotives. Energy 2021;220:119771. https://doi.org/10.1016/j.energy.2021.119771.

[12] Ni M. Thermo-electrochemical modeling of ammonia-fueled solid oxide fuel cells considering ammonia thermal decomposition in the anode. Int J Hydrogen Energy 2011;36(4):3153—66. https://doi.org/10.1016/j.ijhydene.2010.11.100. Elsevier Ltd.

[13] Tukenmez N, Yilmaz F, Ozturk M. A thermal performance evaluation of a new integrated gas turbine-based multigeneration plant with hydrogen and ammonia production. Int J Hydrogen Energy 2020. https://doi.org/10.1016/j.ijhydene.2020.11.054.

[14] Posdziech O, Schwarze K, Brabandt J. Efficient hydrogen production for industry and electricity storage via high-

temperature electrolysis. Int J Hydrogen Energy 2019;4:19089–101. https://doi.org/10.1016/j.ijhydene.2018.05.169.

[15] Aziz M, Putranto A, Biddinika MK, Wijayanta AT. Energy-saving combination of N2 production, NH3 synthesis, and power generation. Int J Hydrogen Energy 2017;42(44):27174–83. https://doi.org/10.1016/j.ijhydene.2017.09.079. Elsevier Ltd.

[16] Hauck M, Herrmann S, Spliethoff H. Simulation of a reversible SOFC with Aspen Plus. Int J Hydrogen Energy 2017;42(15):10329–40. https://doi.org/10.1016/j.ijhydene.2017.01.189. Elsevier Ltd.

[17] O'Brien JE. Thermodynamic considerations for thermal water splitting processes and high temperature electrolysis. In: Proceedings of the ASME international mechanical engineering congress and exposition. Boston, USA. Massachusetts: Idaho National Laboratory (MECE2008 - 68880); 2008. p. 1–13. 31 October-6 November 2008.

[18] Menon V, Janardhanan VM, Deutschmann O. A mathematical model to analyze solid oxide electrolyzer cells (SOECs) for hydrogen production. Chem Eng Sci 2014;110:83–93. https://doi.org/10.1016/j.ces.2013.10.025. Elsevier.

[19] Petipas F, Brisse A, Bouallou C. Model-based behaviour of a high temperature electrolyser system operated at various loads. J Power Sources 2013;239:584–95. https://doi.org/10.1016/j.jpowsour.2013.03.027.

[20] Noren DA, Hoffman MA. Clarifying the Butler-Volmer equation and related approximations for calculating activation losses in solid oxide fuel cell models. J Power Sources 2005;152(1–2):175–81. https://doi.org/10.1016/j.jpowsour.2005.03.174.

[21] Buttler A, Koltun R, Wolf R, Spliethoff H. A detailed techno-economic analysis of heat integration in high temperature electrolysis for efficient hydrogen production. Int J Hydrogen Energy 2015;40(1):38–50. https://doi.org/10.1016/j.ijhydene.2014.10.048. Elsevier Ltd.

[22] Duan C, Kee R, Zhu H, Sullivan N, Zhu L, Bian L, Jennings D, O'Hayre R. Highly efficient reversible protonic ceramic electrochemical cells for power generation and fuel production. Nat Energy 2019;4(3):230–40. https://doi.org/10.1038/s41560-019-0333-2. Springer US.

[23] Ferguson JR, Fiard JM, Herbin R. Three-dimensional numerical simulation for various geometries of solid oxide fuel cells. J Power Sources 1996;58(2):109–22. https://doi.org/10.1016/0378-7753(95)02269-4.

[24] Stephan P, Kabelac S, Kind M, Mewes D, Schaber K, Wetzel T. VDI-Wärmeatlas. 10th ed. Berlin: Springer; 2002.

[25] Nguyen VN, Blum L. Reversible fuel cells. In: Compendium of hydrogen energy. Elsevier; 2016. p. 115–45. https://doi.org/10.1016/B978-1-78242-363-8.00005-0.

[26] Thanganadar D, Asfand F, Patchigolla K. Thermal performance and economic analysis of supercritical Carbon Dioxide cycles in combined cycle power plant'. Appl Energy 2019;255(August):113836. https://doi.org/10.1016/j.apenergy.2019.113836. Elsevier.

[27] Kazempoor P, Braun RJ. Model validation and performance analysis of regenerative solid oxide cells for energy storage applications: reversible operation. Int J Hydrogen Energy 2014;39(11):5955–71. https://doi.org/10.1016/j.ijhydene.2014.01.186. Elsevier Ltd.

[28] Dekker NJJ, Rietveld G. Highly efficient conversion of ammonia in electricity by solid oxide fuel cells. J Fuel Cell Sci Technol 2006;3(4):499–502. https://doi.org/10.1115/1.2349536.

[29] Ma Q, Peng RR, Tian L, Meng G. Direct utilization of ammonia in intermediate-temperature solid oxide fuel cells.

Electrochem Commun 2006;8(11):1791–5. https://doi.org/10.1016/j.elecom.2006.08.012.

[30] Ma Q, Ma J, Zhou S, Yan R, Gao J, Meng G. A high-performance ammonia-fueled SOFC based on a YSZ thin-film electrolyte. J Power Sources 2007;164(1):86–9. https://doi.org/10.1016/j.jpowsour.2006.09.093.

[31] Kazempoor P, Dorer V, Ommi F. Modelling and performance evaluation of solid oxide fuel cell for building integrated co-and polygeneration. Fuel Cell 2010;10(6):1074–94. https://doi.org/10.1002/fuce.200900082.

[32] Ni M, Leung MKH, Leung DYC. Energy and exergy analysis of hydrogen production by solid oxide steam electrolyzer plant. Int J Hydrogen Energy 2007;32(18):4648–60. https://doi.org/10.1016/j.ijhydene.2007.08.005.

[33] Kishimoto M, Muroyama H, Suzuki S, Saito M, Koide T, Takahashi Y, Horiuchi T, Yamasaki H, Matsumoto S, Kubo H, Takahashi N, Okabe A, Ueguchi S, Jun M, Tateno A, Matsuo T, Matsui T, Iwai H, Yoshida H, Eguchi K. Development of 1 kW-class Ammonia-fueled solid oxide fuel cell stack. Fuel Cell 2020;20(1):80–8. https://doi.org/10.1002/fuce.201900131.

[34] Schefold J, Brisse A, Poepke H. Long-term steam electrolysis with electrolyte-supported solid oxide cells. Electrochim Acta 2015;179:161–8. https://doi.org/10.1016/j.electacta.2015.04.141. Elsevier Ltd.

[35] Pinsky R, Sabharwall P, Hartvigsen J, O'Brien J. Comparative review of hydrogen production technologies for nuclear hybrid energy systems. Prog Nucl Energy 2020;123(March):103317. https://doi.org/10.1016/j.pnucene.2020.103317. Elsevier Ltd.

[36] Im-orb K, Visitdumrongkul N, Saebea D, Patcharavorachot Y, Arpornwichanop A. Flowsheet-based model and exergy analysis of solid oxide electrolysis cells for clean hydrogen production. J Clean Prod 2018;170:1–13. https://doi.org/10.1016/j.jclepro.2017.09.127. Elsevier Ltd.

[37] Mogensen MB, Chen M, Frandsen HL, Graves C, Hansen JB, Hansen KV, Hauch A, Jacobsen T, Jensen SH, Skafte TL, Sun X. Reversible solid-oxide cells for clean and sustainable energy. Clean Energy 2019;3(3):175–201. https://doi.org/10.1093/ce/zkz023.

[38] Li M, Brouwer J, Rao AD, Samuelsen GS. Application of a detailed dimensional solid oxide fuel cell model in integrated gasification fuel cell system design and analysis. J Power Sources 2011;196(14):5903–12. https://doi.org/10.1016/j.jpowsour.2011.02.080.

[39] ISPT. TESI115001: power to ammonia, report. Amersfoort: Institute for Sustainable Process Technology; 2017.

[40] Spath PL, Dayton DC. Preliminary screening – technical and economic assessment of synthesis gas to fuels and chemicals with emphasis on the potential for biomass-derived syngas, national renewable energy laboratory. Golden, CO (United States): National Renewable Energy Laboratory; 2003. https://doi.org/10.2172/15006100.

[41] Appl M. Ammonia. In: Ullmann's Encyclopedia of industrial chemistry. Weinheim, Germany: Wiley-VCH Verlag GmbH & Co. KGaA; 2006. https://doi.org/10.1002/14356007.a02_143.pub2.

[42] Pfromm PH. Towards sustainable agriculture: fossil-free ammonia. J Renew Sustain Energy 2017;9(3):034702. https://doi.org/10.1063/1.4985090.

[43] Kitano M, Inoue Y, Sasase M, Kishida K, Kobayashi Y, Nishiyama K, Tada T, Kawamura S, Yokoyama T, Hara M, Hosono H. Self-organized ruthenium-Barium core-shell nanoparticles on a mesoporous calcium amide matrix for efficient low-temperature ammonia synthesis. Angew Chem 2018;130(10):2678–82. https://doi.org/10.1002/ange.201712398.